Low amounts of heavy water increase the phase separation propensity of a fragment of the androgen receptor activation domain

Stasė Bielskutė[¶,1,2], Carla Garcia-Cabau[¶,1,2], Marta Frigolé-Vivas[#,1,2], Elzbieta Szulc[1,2], Eva De Mol[1,2], Mireia Pesarrodona[1,2], Jesús García[1,2] and Xavier Salvatella[*,1,2,3]

[1]Institute for Research in Biomedicine (IRB Barcelona), The Barcelona Institute of Science and Technology, Baldiri Reixac 10, 08028 Barcelona, Spain

[2]Joint BSC-IRB Research Programme in Computational Biology, Baldiri Reixac 10, 08028 Barcelona, Spain

[3]ICREA, Passeig Lluís Companys 23, 08010 Barcelona, Spain

¶ These authors contributed equally

#current address: Dewpoint Therapeutics, Tatzberg 47, 01307 Dresden, Germany

*to whom correspondence should be addressed: xavier.salvatella@irbbarcelona.org

Running title: Effect of heavy water on LLPS

Manuscript details:

Number of manuscript pages: 28

Number of tables: 0

Total number of figures: 5

Number of supplementary material pages: 10

Supplementary material: as supplementary material, we provide a file (bielskute21_supporting_information.pdf) containing 8 figures showing additional DIC microscopy images, NMR data, DLS measurements, turbidity assays and measurements of C_{sat} at different mole fractions of D_2O.

Abstract

The phase equilibria of intrinsically disordered proteins are exquisitely sensitive to changes in solution conditions and this can be used to investigate the driving forces of phase separation *in vitro* as well as the biological roles of phase transitions in live cells. Here we investigate how using D_2O as co-solvent in an aqueous buffer changes the phase equilibrium of a fragment of the activation domain of the androgen receptor, a transcription factor that plays a role in the development of the male phenotype and is a therapeutic target for castration resistant prostate cancer. We show how replacing even small fractions of H_2O with D_2O increases the propensity of this fragment to undergo liquid-liquid phase separation, likely reflecting a stabilization of the hydrophobic interactions that drive condensation. Our results indicate that it is necessary to take this effect into consideration when studying phase separation phenomena with biophysical methods that require using D_2O as a co-solvent. In addition they suggest that additions of D_2O may be used to enhance phase separation phenomena in cells, facilitating their observation.

Keywords: *Liquid-liquid phase separation, LCST, D_2O, NMR, Intrinsically disordered protein, Transcription factor, Androgen receptor.*

Introduction

The formation of biomolecular condensates by liquid-liquid phase separation (LLPS) of intrinsically disordered (ID) proteins is driven by attractive interactions between protein molecules that offset the substantial entropic cost of de-mixing[1]. As a consequence any change in solution conditions that affects the strength of such interactions can shift the phase equilibrium *i.e.* the protein concentration in each liquid phase and, therefore, their relative volume fractions. For example, increases in ionic strength disfavour de-mixing of electrostatic-driven condensates whereas increases in ionic strength will favour the formation of hydrophobic-driven condensates due to the salting out effect. Similarly biomolecular condensation by LLPS can be abolished by high temperature (upper critical solution temperature regime, UCST) when the interactions are enthalpically-driven, as is the case for electrostatic interactions. Instead it can be enhanced by temperature (lower critical solution temperature regime, LCST) when the interactions are entropically driven, as is the case for hydrophobic interactions[2].

It is now well established that phase separation processes are responsible for the formation of cellular organelles that are not surrounded by a membrane, known as membrane-less organelles. It is also likely that highly cooperative but not well-understood phenomena such as chromatin compaction[3] or transcriptional activation[4] also involve phase separation processes. As a consequence of this there is substantial interest in investigating the structural properties of ID proteins in the interior of condensates, rather than in aqueous solution, because the physico-chemical properties of these two environments can be quite different[5]. Specific issues that merit attention include, among others, investigating whether condensation can induce

structure in otherwise ID proteins[6,7] and whether the strength of inter-molecular interactions - including interactions with drug-like molecules - is altered in condensates[8–10]. Answering these questions is important to better understand the roles that condensation plays in the regulation of biological functions and how it can contribute to the onset of disease - for example due to the presence of mutations - as well as to assess whether it will be possible to direct small molecules to therapeutic targets in biomolecular condensates[10].

Biophysical techniques such as nuclear magnetic resonance (NMR) and electron paramagnetic resonance (EPR) spectroscopies are in a good position to contribute to these studies because they have the potential to provide residue-specific structural and dynamical information that is otherwise difficult to obtain. Some pioneering studies in which these techniques have been used have already appeared in the literature[11–13] and it is likely that their number will increase as the amount of biologically and biomedically relevant proteins found to form condensates increases. Given that condensation is quite sensitive to solution conditions it is important to determine whether the sample preparation requirements of specific biophysical techniques can influence the results of experiments. Here we report an analysis of how using D_2O as co-solvent influences the phase equilibrium of a biomedically relevant fragment of the activation domain of a transcription factor, the androgen receptor (AR), that undergoes LCST LLPS; D_2O is often used as co-solvent in biomolecular NMR to correct for fluctuations in field strength as well as in specific EPR applications.

Our results show that the influence of even small amounts of D_2O is substantial, changing the cloud point of the ID protein by more than 10 °C under solution conditions

typical for solution NMR experiments, and that this is likely due to a strengthening of hydrophobic interactions responsible for LCST LLPS. These findings emphasize the need to take this factor into consideration in designing, analyzing and interpreting biophysical experiments where D_2O is used as co-solvent and suggest that D_2O may be used as an enhancer of LCST LLPS *in vitro,* as well as, potentially, in cells, to investigate biomolecular condensation phenomena.

Results

Tau-5, an AR activation domain fragment, undergoes liquid-liquid phase separation in vitro*

To study the effect of solutions conditions on the phase equilibrium of a protein forming biomolecular condensates we used a fragment of the AR activation domain (AD) known as transactivation unit 5 (Tau-5*)[14], that is amenable to biophysical characterization by NMR spectroscopy[14,15]. AR is a nuclear hormone receptor responsible for the development of the male phenotype upon stimulation by androgens. It is composed of globular hormone and DNA binding domains (LBD and DBD, respectively) (Fig. 1A) and a large ID activation domain (AD, residues 1 to 558). Tau-5* is a sub-domain of the AD that is part of activation function 1 (AF-1*) and is considered a therapeutic target for castration resistant prostate cancer, an advanced stage of prostate cancer that is currently incurable[16,17]. Prior to stimulation by androgens, AR forms a diffuse cytosolic complex with Hsp70 that binds to an N-terminal motif (^{23}FQNLF^{27}) in the AD. Androgen binding to the LBD causes an allosteric conformational change in this domain that leads to the formation of a surface patch in the LBD known as activation function 2 (AF-2).

AF-2 has affinity for the ^{23}FQNLF^{27} motif - of the same AR molecule or a different one - and competes out Hsp70, leading to activation[18]. In addition to causing the break-up of the complex with Hsp70, activation is also associated with nuclear translocation, partly due to the androgen-induced inhibition of a nuclear export signal harbored by the LBD[19], and rapid AR multimerization, that can be either cytosolic or nuclear depending on protein levels as well as on the rate of translocation[20–22].

As part of a recent investigation of how cancer-associated mutations in the E3 ubiquitin ligase speckle-type POZ protein (SPOP) affect its ability to co-phase separate with its substrates, including AR, we recently showed that the AR AD is sufficient to undergo LLPS *in vitro*[23]. To determine whether the Tau-5* fragment is also sufficient to undergo LLPS and to compare its LLPS propensity to the full domain, we expressed both constructs as recombinant proteins in *E. coli* and incubated them *in vitro* in a wide range of concentrations and ionic strengths. We observed that Tau-5* indeed undergoes LLPS, as shown in Fig. 1B, forming droplets capable of fusing (Fig. S1). We found however that at equivalent concentrations - in mass per volume units - the AD, composed of 558 residues, has a higher propensity to undergo LLPS than Tau-5*, that contains only 119 residues. At 2.4 mg.mL^{-1}, for example, the AD readily forms condensates whereas Tau-5* hardly does. This observation is in agreement with multivalency being a key driver for LLPS[24] and with the results of molecular simulation of LLPS using coarse grained models[25], that showed how the size of ID proteins influences their propensity to phase separate. In summary, therefore, Tau-5* represents a useful system to investigate how solution conditions affect the phase separation properties of a small TF AD fragment; in addition the fact that this small domain is

amenable to solution NMR spectroscopy makes it possible to use this technique to investigate the potential causes of such effects.

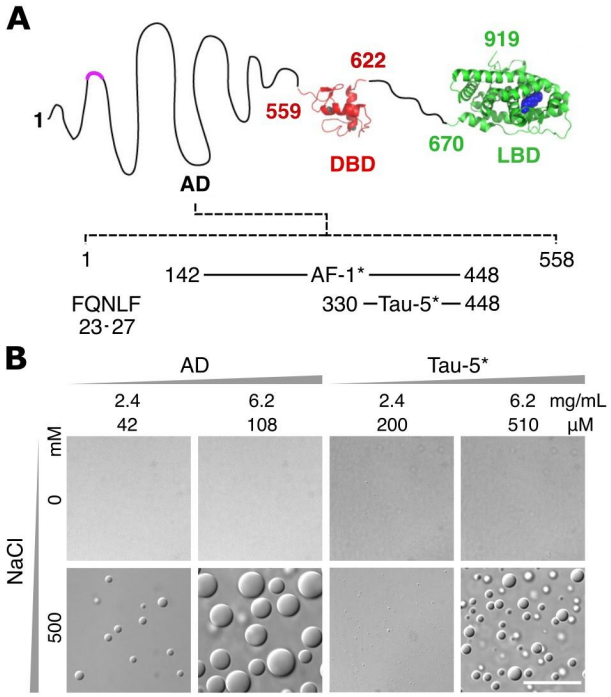

Figure 1. (A) Domain organization of AR with an indication of the position of Zn atoms (grey) in the DBD (red), of dihydrotestosterone (DHT, blue) in the LBD (green), of the binding motif (magenta) of Hsp70 in the AD (black) and defining activation function 1 (AF-1*), the N-terminal motif ^{23}FQNLF^{27} and transcription activation unit 5 (Tau-5*), the region of sequence studied in this work. **(B)** Differential interference contrast (DIC) microscopy images of AD and Tau-5* in the absence and presence of 500 mM NaCl at 25 °C. The scale bar represents 20 µm.

*NMR reveals the oligomerization interface of Tau-5**

To determine whether Tau-5* has propensity to transiently oligomerize prior to undergoing LLPS - and identify the residues involved in stabilizing the putative oligomers as well as the nature of the associated non-covalent interactions - we used

solution NMR under ionic strength and temperature conditions where Tau-5* does not undergo LLPS (Figs. S2 and S3). We carried out ^{1}H,^{15}N-BEST-TROSY experiments at concentrations ranging from 25 to 600 μM and observed that the resonances corresponding to a substantial number of residues experienced small but measurable $^{1}H^{N}$ and ^{15}N chemical shift perturbations as well as decreases in intensity (Fig. 2A), equivalent to those observed for other phase separating ID proteins under conditions where no phase separation is observed[26]. An analysis of the position-dependence of such concentration-dependent changes indicates that they occur in the same residues and with equivalent amplitudes, with the exception of residues flanking the Pro-rich motif at its N-terminus, centered around position 370 (Fig. 2B-D). Indeed this region of sequence shows clear chemical shift changes, as shown in the inset corresponding to L369 in Fig. 2A, but hardly decrease in intensity.

With the goal of better understanding the causes of these effects we investigated which amino acid property best correlated with the behavior observed by NMR. We compared the chemical shift perturbations and intensity decreases with three relevant properties of this sequence: hydrophobicity, residue-specific helical propensity, and the position of residues with aromatic side chains[27] (Tyr, Phe, His, Trp) (Fig. 2C, D). To quantify hydrophobicity we used the average area buried upon folding[28] (AABUF) and for the analysis of the main chain ($^{1}H^{N}$, ^{15}N, $^{13}C\alpha$, $^{13}C\beta$, $^{13}C'$) chemical shifts in terms of helical propensity we used the algorithm δ2D[29] (Fig. 2C, E). We observed that the residues experiencing chemical shift and intensity changes are in the vicinity of aromatic residues with, again as an exception, residues centered at position 370, that flanks a Pro-rich region. In addition, we observed that the size of the spectral changes was largest for the

region of sequence with highest (*ca* 50%) helical propensity, centered at position 400. The importance of secondary structure becomes apparent by comparing the size of the changes observed in the region of sequence that we termed R2 with that of changes in regions R1 and R3[14]: although the number of aromatic residues is similar in all regions the changes are much larger in R2, that has higher helical propensity and where helical conformations place these aromatics in one face of the helix (Fig. 2G).

The concentration-dependence of the chemical shifts indicates that monomeric Tau-5* is in intermediate to fast exchange with oligomeric species present at low population (as shown by DLS measurements, Fig. S3) in which the residues highlighted by the NMR experiments have a chemical shift that is markedly different than the one they have in monomeric Tau-5*. These differences can be due either to changes in chemical environment upon establishment of inter-molecular interactions *i.e.* direct, to conformational changes upon oligomerization *i.e.* indirect, or to a combination of both effects. Although it is likely that the residues undergoing chemical shift changes correspond to those involved in transient oligomerization it is important to consider the complexity of the relationship between protein chemical shifts and protein conformation in the interpretation of these results[30]. In particular the observation that the residues experiencing the largest chemical shift changes are aromatic or in the vicinity of aromatic residues does not necessarily mean that such residues are involved in the establishment of inter-molecular interactions such as π-π or cation-π interactions: it is possible that they are simply particularly good reporters of transient oligomerization due to intra- or inter-molecular ring current effects, that can cause large chemical shifts changes, especially for ^{1}H nuclei.

To obtain a more accurate understanding of direct *vs* indirect effects we measured the changes in ^{13}Cα chemical shift with concentration by using HNCA experiments (Fig. S4A). Indeed ^{13}Cα shifts are more strongly correlated with protein conformation and, specifically, with secondary structure than both $^{1}H^{N}$ and main chain ^{15}N chemical shifts[30]. We observed that ^{13}Cα chemical shift changes can indeed be measured but are very small, lower than 0.1 ppm, even with a 16-fold concentration ratio, indicating that the change of secondary structure upon oligomer formation is very minor (Fig. S4A). Finally the correlation that we observe between $^{1}H^{N}$ and ^{15}N chemical shift changes and decreases in intensity suggests the latter are due to exchange broadening processes associated with transient oligomerization, although it would be necessary to carry out more detailed NMR measurements to determine this unequivocally. Regardless of the interpretation of the NMR results in terms of inter-molecular interactions the linear dependence of chemical shift perturbations with concentration indicates that the oligomerization equilibrium of Tau-5* is shifted to the monomer, *i.e.* that the population of oligomers is low, in agreement with the results obtained by DLS (Fig. S3) and that Tau-5* molecules populate the oligomeric state only transiently (Fig. 2F). We conclude, therefore, that Tau-5* has a clear, albeit weak, propensity to oligomerize, that the oligomers are, like those involved in TDP-43 LLPS[26], stabilized by interactions between residues in a partially folded helix (Fig. 2G), that the secondary structure in the oligomers is likely similar to that of the monomers and that the inter-molecular interactions could include π-π or cation-π interactions (Fig. 2H).

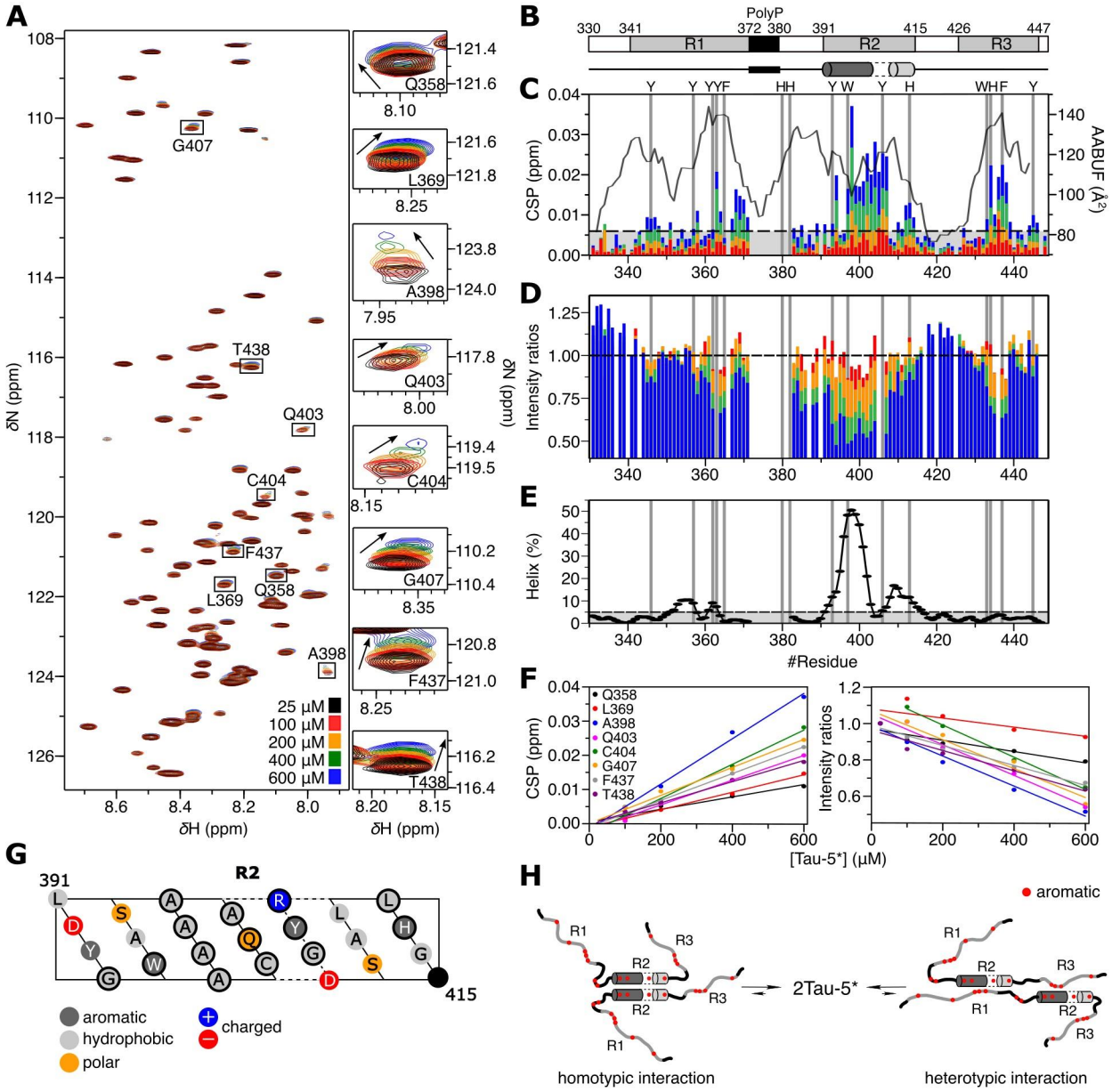

Figure 2. NMR analysis of Tau-5* at different concentrations. **(A)** Overlay of $^{1}H,^{15}N$-BEST-TROSY spectra of Tau-5* at increasing concentrations. The resonances corresponding to residues Q358, L369, A398, Q403, C404, G407, F437 and T438 are shown separately to highlight their concentration-dependence. **(B)** Indication of the R1, R2, R3 regions and secondary structure[14]. **(C)** Combined $^{1}H^{N}$ and ^{15}N chemical shift perturbations (CSP) caused by increases in Tau-5* concentration, relative to the value measured at 25 μM, as a function of residue number, with an indication of the hydrophobicity of the sequence, in terms of AABUF[28]. The dashed line indicates the experimental error (0.006 ppm). **(D)** Ratio of normalized NMR

intensities ($I^n_{100\text{-}600\mu M}/I^n_{25\mu M}$) obtained from the $^1H,^{15}N$-BEST-TROSY spectra shown in panel A. **(E)** Helical propensity of Tau-5* at 25 μM as obtained from an analysis of NMR chemical shifts ($^1H^N$, ^{15}N, $^{13}C\alpha$, $^{13}C\beta$, $^{13}C'$) by using the algorithm δ2D[29]. The horizontal dashed line indicates the uncertainty of the algorithm (5 %). **(F)** CSP and ratio of normalized intensities for residues Q358, L369, A398, Q403, C404, G407, F437 and T438. **(G)** Helix projection of R2 (391-414). Two motifs with distinct helical propensity are connected by an essentially disordered stretch of sequence, indicated by a dashed line. Black stroke paint indicates residues with CSP above 0.01 ppm value in panel A. **(H)** Schematic representation of intermolecular interactions between two Tau-5* molecules. The color code used for each protein concentration is displayed in panel A and is the same for all panels of the figure. Vertical grey lines in panels C-E indicate the position of aromatic residues in the sequence.

As shown in Fig. 1B ionic strength has a strong impact on the propensity of both Tau-5* and the AD to condensate. To investigate whether the oligomerization process characterized by NMR is, at least in part, responsible for condensation, we investigated the effect of increases in salt concentration (additions of 100, 200 and 300 mM NaCl) on the NMR spectrum of 400 μM Tau-5*. We observed that, at constant Tau-5* concentration, increasing NaCl concentration causes changes in $^1H^N$ and ^{15}N chemical shifts as well as decreases in signal intensity (Figs. 3A, B and S5). The changes in chemical shift (Fig. 3A, bottom) were difficult to interpret: although in R3, for example, they are similar to those caused by increases in Tau-5* concentration (Fig. 3A, top), suggesting a shift in the oligomerization equilibrium, this is not the case for regions R1 and R2. For R2 they appear to correlate with AABUF whereas in R1 the opposite holds. These apparent discrepancies are likely due to a convolution of the various effects that changes in ionic strength can have on main chain resonances, that include changes in side chain conformation, changes in secondary structure caused by electrostatic interactions between side chains, changes in oligomerization propensity, etc. Indeed,

the fact that R3, where chemical shift changes suggest a shift in oligomerization equilibrium, contains a relatively low number of charged side chains (2 for R3 vs 3 for R2 and 5 for R1) is in agreement with this possibility (Fig. 3C). The analysis of the changes in $^{13}C\alpha$ chemical shifts was also challenging: although the changes in R3 indicate a small enhancement of helical propensity the results in the rest of the sequence seem to be affected by other changes that cannot be easily attributed to shifts in the oligomerization equilibrium (Fig. S4B).

The changes in signal intensity induced by increases in the NaCl concentration at constant Tau-5* concentration were by contrast easier to interpret. As shown in Fig. 3B (bottom) decreases in signal intensity upon increase in NaCl concentration are essentially the same, both in terms of the residues involved and in terms of their amplitude, than upon changes of Tau-5* concentration at constant ionic strength (top). This clearly indicates that increases in ionic strength enhance Tau-5* oligomerization, which is in agreement with the hypothesis that such interactions contribute to Tau-5* condensation at the appropriate solution conditions. We conclude, therefore, that NMR experiments can be used to detect shifts in the oligomerization equilibrium of Tau-5* as a consequence of changes in solution conditions and that this technique reveals that the oligomerization interface is likely rich in aromatic residues involved in hydrophobic and, potentially, cation-π and π-π interactions.

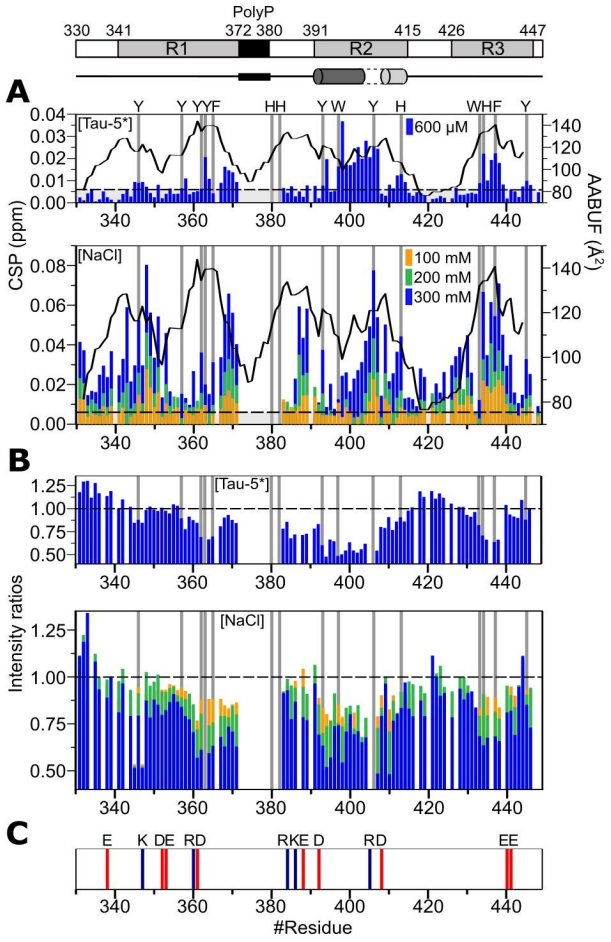

Figure 3. Comparison of Tau-5* CSP and normalized intensities between different protein concentrations and ionic strengths as a function of residue number. **(A)** CSP upon increasing protein concentration from 25 to 600 µM (top), and upon increasing the ionic strength (reference 0 mM NaCl) at a given Tau-5* concentration (400 µM) (bottom). Dashed lines represent experimental errors. **(B)** Ratio of normalized intensities of Tau-5* at 600 and 25 µM ($I^n_{600\mu M}/I^n_{25\mu M}$) (top), and at different ionic strengths (reference 0 mM NaCl) at 400 µM Tau-5* (bottom). **(C)** Distribution of charged residues in the Tau-5* sequence. Positively and negatively charged residues are labeled in blue and red, respectively.

Condensation is enhanced by strengthening hydrophobic interactions

Given the results of our NMR experiments, that revealed a hydrophobic oligomerization interface in Tau-5* and an associated enhancement of oligomerization upon increases in ionic strength, we hypothesized that Tau-5* would condensate under the LCST regime. To confirm this we studied the light scattering properties of a 200 µM Tau-5* sample with 400 mM NaCl by measuring the apparent absorbance in a cuvette spectrophotometer as a function of temperature with a heating rate of $1°C \cdot s^{-1}$. We observed, in agreement with our hypothesis, that condensation only occurred upon heating, with a cloud point of 37 °C (Fig. 4A, black curve). However, upon preparation of an NMR sample under conditions that should, according to this result, not lead to condensation we observed, surprisingly, that addition of D_2O caused a clear increase of turbidity, suggesting that this co-solvent may alter the phase equilibrium of Tau-5* (data not shown). To quantify this effect we carried out additional cloud point measurements and observed that even small additions of D_2O caused a marked decrease in the cloud point (Fig. 4B) corresponding to an increase of condensation propensity. The shift was approximately linear, of *ca* 0.5 °C for each percentage point in D_2O, meaning that additions of 5 to 10% D_2O, as is customary in solution NMR, can lead to cloud point shifts in the order of up to 5 °C, suggesting a substantial alteration of the phase equilibrium.

Cloud point measurements such as those reported in Fig. 4A are very useful to readily detect apparent changes in phase diagrams but do not represent equilibrium measurements. It is conceivable that additions of co-solvents or other perturbations, such as mutations, could change the cloud point not by changing the phase equilibrium

but, rather, by changing the rate at which the condensates build-up. Therefore, to complement the results presented in Fig. 4A we carried out equilibrium experiments, at a constant temperature of 25 ºC, where we analyzed by differential interference contrast (DIC) optical microscopy a solution of 200 μM Tau-5* with 400 mM NaCl. In aqueous buffer we observed a single phase but at D_2O percentages of *ca* 30% and above we observed the formation of Tau-5* droplets, with a size that increased with D_2O percentage (Fig. 4C). This indicates that the volume fraction of condensate increases as D_2O is added, indicating that the shift in phase equilibrium - in terms of volume fractions - indeed occurs. Finally we measured the saturation concentration for LLPS, i.e. the concentration of Tau-5* in the supernatant after separation of the two liquid phases by centrifugation, obtaining that it decreases with the fraction of H_2O replaced by D_2O (Fig. S6).

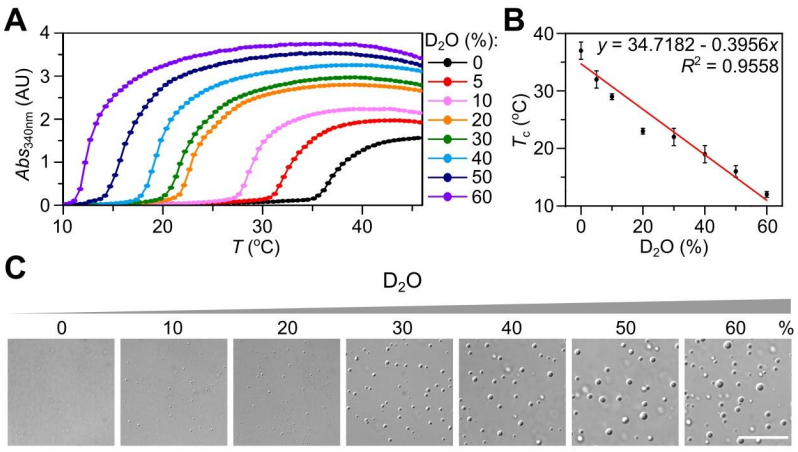

Figure 4. Effect of using D_2O as co-solvent on the cloud point of Tau-5*. **(A)** Apparent absorbance at 340 nm of a solution of 200 μM Tau-5* at 400 mM NaCl as a function of temperature at increasing percentages of D_2O. **(B)** Cloud points obtained from panel A. **(C)** DIC images at 25 ºC at increasing mole fractions of D_2O. Scale bar represents 20 μm.

The surprisingly large effect that D_2O addition has on the phase equilibrium of Tau-5* calls for an investigation of its causes. The NMR experiments reported in Figs. 2 and 3 proved useful to attribute the increase in condensation propensity to a likely strengthening of hydrophobic interactions between residues in the oligomerization interface, that is rich in hydrophobic and aromatic residues. We thus used the same approach to investigate the effect of increasing the percentage of D_2O on the main chemical shifts of Tau-5* at constant concentration (400 μM) and in the absence of NaCl (Figs. 5 and S4C). We found that at 20% D_2O the chemical shift changes were small, almost not significant, but that at 30% D_2O they became quite large, especially in residues which experienced largest chemical shift changes upon increases in Tau-5* concentration (Figs. 5 and S7). At 50% D_2O we found that the changes in chemical shift were widespread but still stronger in residues that are part of the oligomerization interface. This result indicates that D_2O shifts the oligomerization equilibrium similarly as an increase in Tau-5* concentration, that is that D_2O strengthens the interactions that govern the oligomerization equilibrium, thus explaining the striking effect that this co-solvent has on the LLPS equilibrium of Tau-5*.

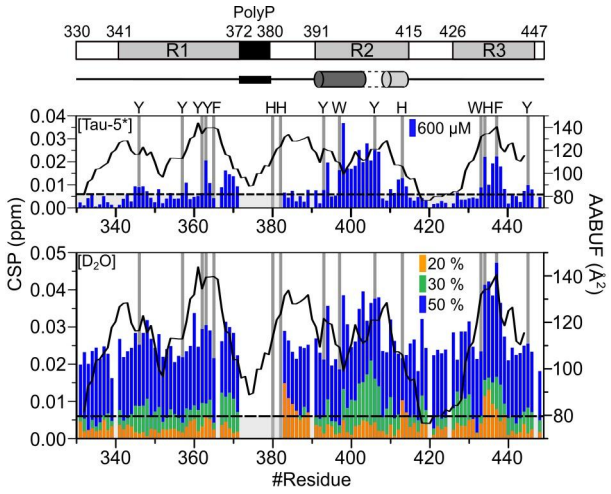

Figure 5. Comparison of Tau-5* CSP induced upon increases in protein concentration (top) and D_2O percentage (bottom). CSP upon increasing Tau-5* concentration from 25 to 600 μM (top), and upon increasing D_2O percentage (reference 10 % D_2O) of 400 μM Tau-5* (bottom). Dashed lines represent experimental errors.

Discussion

Our results indicate that even modest molar fractions of D_2O in a buffer solution can have a substantial effect on the phase diagram of a protein undergoing LCST LLPS. We attribute this to a strengthening of hydrophobic interactions, a phenomenon that had already been observed both in protein folding[31] and aggregation studies[32,33], that is mainly due to a strengthening of solvent-solvent interactions upon deuteration. The sign of the effect *i.e.* that LCST LLPS is enhanced by heavy water is therefore not a particularly surprising result but the amplitude of the effect, instead, is: we note that the majority of above mentioned studies examined the consequences of replacing H_2O with D_2O, obtaining measurable but small changes, whereas here we show changes in cloud point as large as 25 ºC upon replacement of 50% H_2O with D_2O, that represents a very profound alteration of the phase diagram of an ID protein.

It will be interesting to study to what extent this phenomenon is general or whether it is a peculiarity of the construct studied here. It will be important to determine, for example, whether the phase diagram of proteins that form condensates stabilized by interactions other than hydrophobic, undergoing UCST LLPS, show a similar behavior. Similarly it will be necessary to determine how this effect scales with protein size and with specific sequence features such as presence and patterning of aromatic and charged residues,

secondary structure propensity and, in essence, any of the sequence features that influence phase separation propensity[1]. Finally, in analogy with protein folding studies, it will also be interesting to investigate how the use of co-solvents other than D_2O, that modify the strength of inter-molecular interactions or the structural properties of ID proteins, alter their phase separation properties[34].

1,6-hexanediol is often used both *in vitro* but especially in live cells to investigate phase separation phenomena. This compound is thought to destabilize biomolecular condensates formed by hydrophobic interactions and, as a consequence, the loss of puncti and of specific biological activities upon 1,6-hexanediol addition is often put forward as evidence of LLPS-mediated phenomena[4,35]. It is however possible that addition of this alcohol can cause different effects, ranging from alterations of membrane structure to changes in the stability of the structures of globular proteins. Indeed, it has been recently shown that percentages of 1,6-hexanediol commonly used to disrupt LLPS impact enzymatic activity, for example, inactivating kinases and phosphatases[36]. It is therefore necessary to develop new probes to selectively change the stability of condensates: since moderate (up to 70%) mole fractions of D_2O can be tolerated by live cells[37], for example in studies of the rate protein synthesis in physiology[38], analysis of how additions of this co-solvent influence apparent phase separation phenomena in cells may represent a useful tool in this field.

Material and methods

Protein expression and purification

The DNA sequences coding for human AR AD (polyQ58-78 and plyG449-472 tracts) residues 1 to 558 (AD) and 330 to 448 (Tau-5*) were cloned into Gateway pDEST17 vectors (Invitrogen) with N-terminal His6-tag, TEV and 3C cleavage sites, respectively. Transformed *E. coli Rosetta* cells were grown at 37 ^{o}C in LB medium for the production of non isotopically labeled proteins. For single (^{15}N) or double (^{15}N,^{13}C) isotopic labeling cells were grown in M9 minimal medium containing $^{15}NH_4Cl$ or $^{15}NH_4Cl$ and ^{13}C-glucose, respectively.

Protein expression was induced at OD (600 nm) = 0.7 with 1 mM IPTG and cells were cultured at 25 °C overnight. Cells were harvested by centrifugation at 4,500 r.p.m. for 15 mins and resuspended in a phosphate buffered saline (PBS), containing 0.05 % NaN_3. Cells were disrupted twice by sonication for 6 mins at 38% intensity with a pulse 5 sec on and 5 sec off. Supernatants were discarded by centrifugation at 20,000 r.p.m. for 45 mins and the pellets were washed twice with a wash buffer (PBS, 1 % Triton, 500 mM NaCl, 1 mM DTT, pH 7.8). Insoluble inclusion bodies were collected by centrifugation at 20,000 r.p.m for 45 mins and solubilized in a binding buffer (20 mM Tris, 500 mM NaCl, 5 mM imidazole, 8 M urea, 0.05 NaN_3, 1 mM DTT, pH 7.8) at RT overnight.

Solubilized inclusion bodies were centrifuged at 20,000 r.p.m. for 45 mins and the supernatant filtered and applied to a 5 mL HisTrap HP column (GE healthcare) at RT. Samples were eluted from the column using a gradient of 500 mM imidazole in the binding buffer. Samples were then dialysed twice in a dialysis buffer (50 mM Tris, 1 mM DTT, 0.5 mM EDTA, pH 8.0). His_6-tag of AD and Tau-5* were cleaved by TEV and 3C proteases, respectively, which were added in the second step of the dialysis. 8 M urea was added in the cleaved samples and samples were filtered. The proteins obtained by proteolytic cleavage were separated from the tags by reverse Ni^{2+} affinity.

The proteins were concentrated using 3,000 MWCO 15 mL Amicon centrifugal filters, filtered using sterile 0.22 µm filters and stored at -80 °C in the binding buffer.

Sample preparation

Immediately before each measurement, frozen protein solutions were thawed on ice and a buffer exchange step was employed using a Superdex 200 column (GE healthcare) at 4 °C, equilibrated in a

buffer containing 20 mM NaP, pH 7.4, 1 mM TCEP, 0.05 % NaN_3. The protein-containing fractions were concentrated using a 3,000 MWCO 4 mL Amicon centrifugal filter by centrifugation at 4,000 r.p.m. at 4 °C. The concentrated proteins were centrifuged for 20 mins at 15,000 r.p.m. at 4 ºC, and the supernatant was used for sample preparation. The concentrations were determined by measuring UV absorbance at 280 nm, using extinctions coefficients of 55405 and 21555 $M^{-1}cm^{-1}$ for AD and Tau-5*, respectively.

All samples for experiments were prepared on ice. The indicated percentages of D_2O in the samples was achieved by adding a fully deuterated equivalent buffer, containing 20 mM NaP, pH 7.4, 1 mM TCEP, 0.05 % NaN_3, and NaCl was added from a 5 M aqueous solution. The pH of both stocks was adjusted to 7.4 and filtered using sterile 0.22 µm filters before being used for samples preparation. For samples with different D_2O percentages, no additional pH correction was applied (all samples pH 7.4), considering that no correction is needed for the p(H,D) measurement when comparing it to pH^H for any D_2O content, if $4 < p(H,D) < 8$[39]. Additionally, we carried out turbidity experiments to confirm that changes in pH by 0.2 (from pH 7.4 to 7.6) units do not influence LLPS of Tau-5* (Fig. S8).

NMR samples additionally contained 10 µM DSS and 10 % D_2O (unless otherwise stated). A higher percentage of D_2O than 10 % for NMR samples was achieved by adding a fully deuterated equivalent buffer. After mixing the components, the pH was checked again before the NMR measurements.

DLS samples were additionally centrifuged for 5 mins at 15,000 r.p.m. at 4 ºC and the resulting supernatant was used for the measurement.

Differential interference contrast (DIC) microscopy

All samples were prepared as described in the section of Sample preparation. For each condition, 1.2 µL of sample was deposited in a sealed chamber comprising a slide and a coverslip sandwiching double sided tape (3M 300 LSE high-temperature double-sided tape of 0.17 mm thickness). The used coverslips were previously coated with PEG-silane following a published protocol[40]. The DIC images were taken using an automated inverted Olympus IX81 microscope with a 60x/1.42 oil Plan APo N objective using the Xcellence rt 1.2 software.

Turbidity assay

Turbidity assays were performed on a Cary 100 UV-Vis spectrophotometer equipped with a multicell thermoelectric temperature controller using 1 cm path length cells. Samples were heated at a rate of 1 °C.min^{-1} in the range 10 to 60 °C and apparent absorbance at 340 nm was monitored as a function of temperature. Cloud points (T_c) of LLPS were determined as the maximum of the derivative of the plot of *Abs* (340 nm) versus *T*. Uncertainties of T_c were determined from comparison of 3 identical experiments.

NMR

NMR spectra were recorded at 278 K on a 800 MHz Bruker Avance NEO spectrometer equipped with a TCI cryoprobe. Combined $^{1}H^{N}$ and ^{15}N chemical shift perturbations were obtained from ^{1}H,^{15}N-BEST-TROSY experiments and calculated using the following equation:

$$CSP = \sqrt{(\delta H_2 - \delta H_1)^2 + (\frac{\delta N_2 - \delta N_1}{5})^2}$$

$^{13}C\alpha$, $^{13}C\beta$ and $^{13}C'$ chemical shifts were obtained from the BEST-TROSY version of 3D HNCA, HNCO and HNcoCACB experiments acquired with NUS.

Data processing was carried out with qMDD[41] for non-uniform sampled data and NMRPipe[42] for all uniformly collected experiments.

Data analysis was performed with CcpNMR analysis[43]. All spectra were referenced directly using DSS for the ^{1}H dimension. ^{13}C and ^{15}N frequencies were referenced indirectly. Uncertainties of CSP and $\Delta^{13}C\alpha$ were determined from comparison of 3 identical experiments.

Measurement of C_{sat}

After Tau-5* condensation, samples were incubated for 5 mins at 25 °C followed by centrifugation at 2,000 r.p.m. for 2 mins at 25 °C. The concentration of Tau-5* in the supernatant, C_{sat}, was determined by UV spectroscopy. Uncertainties of C_{sat} were determined from comparison of 3 identical experiments.

Dynamic light scattering (DLS)

The DLS measurements were taken with a Zetasizer Nano-S instrument (Malvern) equipped with a He-Ne of 633 nm wavelength laser. Three measurements were performed for each sample, each of the measurements consisting of 10 runs of 10 s each. The experiments were carried out at 5 °C.

Acknowledgements

S.B. acknowledges a PhD fellowship awarded by IRB in the 2020 call. C.G. acknowledges an FPI fellowship awarded by MINECO in the 2018 call. M.F., E.S. and E.D.M acknowledge PhD fellowships awarded by “la Caixa” foundation. X.S. acknowledges funding from AGAUR (2017 SGR 324), MINECO (BIO2015-70092-R) and the European Research Council (CONCERT, contract number 648201). The authors thankfully acknowledge the NMR resources and the technical support provided by the LRB of the Spanish ICTS Red de Laboratorios de RMN de biomoléculas (R-LRB). The authors thankfully acknowledge the IRB Barcelona Advanced Digital Microscopy (ADM) Core Facility, in particular Anna Lladó, for their help and support regarding microscopy experiments. IRB Barcelona is the recipient of a Severo Ochoa Award of Excellence from MINECO (Government of Spain).

References

1. Martin EW, Mittag T (2018) Relationship of Sequence and Phase Separation in Protein Low-Complexity Regions. Biochemistry 57:2478–2487.

2. Ruff KM, Roberts S, Chilkoti A, Pappu RV (2018) Advances in Understanding Stimulus-Responsive Phase Behavior of Intrinsically Disordered Protein Polymers. J. Mol. Biol. 430:4619–4635.

3. Gibson BA, Doolittle LK, Schneider MWG, Jensen LE, Gamarra N, Henry L, Gerlich DW, Redding S, Rosen MK (2019) Organization of Chromatin by Intrinsic and Regulated Phase Separation. Cell 179:470–484.e21.

4. Boija A, Klein IA, Sabari BR, Dall’Agnese A, Coffey EL, Zamudio AV, Li CH, Shrinivas K, Manteiga JC, Hannett NM, et al. (2018) Transcription Factors Activate Genes through the Phase-Separation Capacity

of Their Activation Domains. Cell 175:1842–1855.e16.

5. Nott TJ, Craggs TD, Baldwin AJ (2016) Membraneless organelles can melt nucleic acid duplexes and act as biomolecular filters. Nat. Chem. 8:569–575.

6. Lin Y-H, Brady JP, Forman-Kay JD, Chan HS (2017) Charge pattern matching as a “fuzzy” mode of molecular recognition for the functional phase separations of intrinsically disordered proteins. New J. Phys. 19:115003.

7. Lin Y-H, Song J, Forman-Kay JD, Chan HS (2017) Random-phase-approximation theory for sequence-dependent, biologically functional liquid-liquid phase separation of intrinsically disordered proteins. J. Mol. Liq. 228:176–193.

8. Klein IA, Boija A, Afeyan LK, Hawken SW, Fan M, Dall’Agnese A, Oksuz O, Henninger JE, Shrinivas K, Sabari BR, et al. (2020) Partitioning of cancer therapeutics in nuclear condensates. Science 368:1386–1392.

9. Wheeler RJ (2020) Therapeutics-how to treat phase separation-associated diseases. Emerg Top Life Sci [Internet]. Available from: http://dx.doi.org/10.1042/ETLS20190176

10. Biesaga M, Frigolé-Vivas M, Salvatella X (2021) Intrinsically disordered proteins and biomolecular condensates as drug targets. Curr. Opin. Chem. Biol. 62:90–100.

11. Ambadipudi S, Reddy JG, Biernat J, Mandelkow E, Zweckstetter M (2019) Residue-specific identification of phase separation hot spots of Alzheimer’s-related protein tau. Chem. Sci. 10:6503–6507.

12. Murthy AC, Dignon GL, Kan Y, Zerze GH, Parekh SH, Mittal J, Fawzi NL (2019) Molecular interactions underlying liquid-liquid phase separation of the FUS low-complexity domain. Nat. Struct. Mol. Biol. 26:637–648.

13. Burke KA, Janke AM, Rhine CL, Fawzi NL (2015) Residue-by-Residue View of In Vitro FUS Granules that Bind the C-Terminal Domain of RNA Polymerase II. Mol. Cell 60:231–241.

14. De Mol E, Fenwick RB, Phang CTW, Buzón V, Szulc E, de la Fuente A, Escobedo A, García J,

Bertoncini CW, Estébanez-Perpiñá E, et al. (2016) EPI-001, A Compound Active against Castration-Resistant Prostate Cancer, Targets Transactivation Unit 5 of the Androgen Receptor. ACS Chem. Biol. 11:2499–2505.

15. De Mol E, Szulc E, Di Sanza C, Martínez-Cristóbal P, Bertoncini CW, Fenwick RB, Frigolé-Vivas M, Masín M, Hunter I, Buzón V, et al. (2018) Regulation of Androgen Receptor Activity by Transient Interactions of Its Transactivation Domain with General Transcription Regulators. Structure 26:145–152.e3.

16. Christiaens V, Bevan CL, Callewaert L, Haelens A, Verrijdt G, Rombauts W, Claessens F (2002) Characterization of the two coactivator-interacting surfaces of the androgen receptor and their relative role in transcriptional control. J. Biol. Chem. 277:49230–49237.

17. Jenster G, van der Korput HA, Trapman J, Brinkmann AO (1995) Identification of two transcription activation units in the N-terminal domain of the human androgen receptor. J. Biol. Chem. 270:7341–7346.

18. Eftekharzadeh B, Banduseela VC, Chiesa G, Martínez-Cristóbal P, Rauch JN, Nath SR, Schwarz DMC, Shao H, Marin-Argany M, Di Sanza C, et al. (2019) Hsp70 and Hsp40 inhibit an inter-domain interaction necessary for transcriptional activity in the androgen receptor. Nat. Commun. 10:1–14.

19. Saporita AJ, Zhang Q, Navai N, Dincer Z, Hahn J, Cai X, Wang Z (2003) Identification and Characterization of a Ligand-regulated Nuclear Export Signal in Androgen Receptor*. J. Biol. Chem. 278:41998–42005.

20. Black BE, Paschal BM (2004) Intranuclear organization and function of the androgen receptor. Trends Endocrinol. Metab. 15:411–417.

21. Tomura A, Goto K, Morinaga H, Nomura M, Okabe T, Yanase T, Takayanagi R, Nawata H (2001) The subnuclear three-dimensional image analysis of androgen receptor fused to green fluorescence protein. J. Biol. Chem. 276:28395–28401.

22. Kumar S, Tyagi RK (2012) Androgen receptor association with mitotic chromatin--analysis with introduced deletions and disease-inflicting mutations. FEBS J. 279:4598–4614.

23. Bouchard JJ, Otero JH, Scott DC, Szulc E, Martin EW, Sabri N, Granata D, Marzahn MR, Lindorff-Larsen K, Salvatella X, et al. (2018) Cancer Mutations of the Tumor Suppressor SPOP Disrupt the Formation of Active, Phase-Separated Compartments. Mol. Cell 72:19–36.

24. Li P, Banjade S, Cheng H-C, Kim S, Chen B, Guo L, Llaguno M, Hollingsworth JV, King DS, Banani SF, et al. (2012) Phase transitions in the assembly of multivalent signalling proteins. Nature 483:336–340.

25. Dignon GL, Zheng W, Kim YC, Best RB, Mittal J (2018) Sequence determinants of protein phase behavior from a coarse-grained model. PLoS Comput. Biol. 14:e1005941.

26. Conicella AE, Zerze GH, Mittal J, Fawzi NL (2016) ALS Mutations Disrupt Phase Separation Mediated by α-Helical Structure in the TDP-43 Low-Complexity C-Terminal Domain. Structure 24:1537–1549.

27. Martin EW, Holehouse AS, Peran I, Farag M, Incicco JJ, Bremer A, Grace CR, Soranno A, Pappu RV, Mittag T (2020) Valence and patterning of aromatic residues determine the phase behavior of prion-like domains. Science 367:694–699.

28. Rose GD, Geselowitz AR, Lesser GJ, Lee RH, Zehfus MH (1985) Hydrophobicity of amino acid residues in globular proteins. Science 229:834–838.

29. Camilloni C, De Simone A, Vranken WF, Vendruscolo M (2012) Determination of secondary structure populations in disordered states of proteins using nuclear magnetic resonance chemical shifts. Biochemistry 51:2224–2231.

30. Neal S, Nip AM, Zhang H, Wishart DS (2003) Rapid and accurate calculation of protein 1H, 13C and 15N chemical shifts. J. Biomol. NMR 26:215–240.

31. Parker MJ, Clarke AR (1997) Amide backbone and water-related H/D isotope effects on the dynamics of a protein folding reaction. Biochemistry 36:5786–5794.

32. Chakrabarti G, Kim S, Gupta ML Jr, Barton JS, Himes RH (1999) Stabilization of tubulin by deuterium oxide. Biochemistry 38:3067–3072.

33. Panda D, Chakrabarti G, Hudson J, Pigg K, Miller HP, Wilson L, Himes RH (2000) Suppression of

microtubule dynamic instability and treadmilling by deuterium oxide. Biochemistry 39:5075–5081.

34. Hamada D, Chiti F, Guijarro JI, Kataoka M, Taddei N, Dobson CM (2000) Evidence concerning rate-limiting steps in protein folding from the effects of trifluoroethanol. Nat. Struct. Biol. 7:58–61.

35. Molliex A, Temirov J, Lee J, Coughlin M, Kanagaraj AP, Kim HJ, Mittag T, Taylor JP (2015) Phase separation by low complexity domains promotes stress granule assembly and drives pathological fibrillization. Cell 163:123–133.

36. Düster R, Kaltheuner IH, Schmitz M, Geyer M (2021) 1,6-Hexanediol, commonly used to dissolve liquid-liquid phase separated condensates, directly impairs kinase and phosphatase activities. J. Biol. Chem. 296:100260.

37. Kushner DJ, Baker A, Dunstall TG (1999) Pharmacological uses and perspectives of heavy water and deuterated compounds. Can. J. Physiol. Pharmacol. 77:79–88.

38. Miller BF, Reid JJ, Price JC, Lin H-JL, Atherton PJ, Smith K (2020) CORP: The use of deuterated water for the measurement of protein synthesis. J. Appl. Physiol. 128:1163–1176.

39. Rubinson KA (2017) Practical corrections for p(H,D) measurements in mixed H2O/D2O biological buffers. Anal. Methods 9:2744–2750.

40. Alberti S, Saha S, Woodruff JB, Franzmann TM, Wang J, Hyman AA (2018) A User's Guide for Phase Separation Assays with Purified Proteins. Journal of Molecular Biology [Internet] 430:4806–4820. Available from: http://dx.doi.org/10.1016/j.jmb.2018.06.038

41. Orekhov VY, Jaravine VA (2011) Analysis of non-uniformly sampled spectra with multi-dimensional decomposition. Prog. Nucl. Magn. Reson. Spectrosc. 59:271–292.

42. Delaglio F, Grzesiek S, Vuister GW, Zhu G, Pfeifer J, Bax A (1995) NMRPipe: a multidimensional spectral processing system based on UNIX pipes. J. Biomol. NMR 6:277–293.

43. Vranken WF, Boucher W, Stevens TJ, Fogh RH, Pajon A, Llinas M, Ulrich EL, Markley JL, Ionides J, Laue ED (2005) The CCPN data model for NMR spectroscopy: development of a software pipeline.

Proteins 59:687–696.